Available online at www.sciencedirect.com
SCIENCE DIRECT
Journal of Catalysis 234 (2005) 88–95
JOURNAL OF CATALYSIS
www.elsevier.com/locate/jcat

Surface-structure sensitivity of CO oxidation over polycrystalline ceria powders

Eleonora Aneggi [a], Jordi Llorca [b], Marta Boaro [a], Alessandro Trovarelli [a,*]

[a] *Dipartimento di Scienze e Tecnologie Chimiche, via del Cotonificio 108, Università di Udine, 33100 Udine, Italy*
[b] *Departament de Quimica Inorganica, Universitat de Barcelona, Martí i Franquès 1-11, 08028 Barcelona, Spain*

Received 18 April 2005; revised 27 May 2005; accepted 9 June 2005

Available online 14 July 2005

Abstract

In this study a series of CeO_2 powders with surface area in the range of 10–140 m^2/g were prepared by calcination at increasing temperatures of samples of polycrystalline ceria and used as catalysts for CO oxidation under a free diffusion limitation regime. It was found that aging under air of polycrystalline ceria samples, regardless of the preparation method used, caused the rearrangement of crystallites, with loss of surface area and exposure of more reactive surfaces, which increases the specific activity in CO oxidation. HRTEM analysis has shown that the treatment under oxygen at temperatures greater than 773 K results in the truncation of the sharp tips between two {111}-type surfaces, exposing new and more reactive surfaces of the {100} type. In accordance with previous theoretical calculations and with recent studies on monodimensional ceria samples, a correlation between exposure of these surfaces and an increase in specific reaction rate was found.

Keywords: Ceria; CeO_2; CO oxidation; Structure sensitivity

1. Introduction

Cerium dioxide is a key component in the formulation of several commercial catalysts. Its major use is as a promoter in the catalysts used for reducing CO, hydrocarbons, and NO_x emissions from gasoline engines, where it acts as an oxygen storage/release medium that is continuously reduced and oxidized under cycling feedstream conditions [1,2]. A complex series of redox reactions occurs on the ceria surface in the presence of lean/rich gas mixtures, which involve continuous formation and annihilation of oxygen vacancies and changes in the redox state of cerium (IV/III). CO oxidation is one of the key steps in the overall process, and therefore it has frequently been used as a probe reaction over ceria-based materials to evaluate different catalyst formulations and investigate mechanistic issues [3–7]. It is generally accepted that CO oxidation under stationary conditions occurs over pure ceria by a Mars–van Krevelen-type mechanism, where reaction involves alternate reduction and oxidation of the ceria surface with formation of surface oxygen vacancies (as the key step) and their successive replenishment by gas-phase oxygen. Therefore an understanding of the structure and relative stability of the surfaces of CeO_2 can provide useful insights closely related to catalytic reactions that normally take place on these surfaces. A few theoretical studies have investigated the structure and relative stability of surfaces of CeO_2, and the results have indicated that the compact {111} surfaces are the most stable (and are therefore less reactive), followed by {110}, {100}, and {211} [8–10]. It has recently been reported that materials with 1D-like morphology specifically prepared to predominantly expose these planes are more reactive than conventionally prepared cerium oxide in CO oxidation [11]. Although in this case comparison of activity has been made on the basis of light-off curves only, it was shown that 1D materials in the form of nanorods exposing {100} and {110} planes

* Corresponding author. Fax: +39-0432-558803.
E-mail address: trovarelli@uniud.it (A. Trovarelli).

0021-9517/$ – see front matter
doi:10.1016/j.jcat.2005.06.008

have a higher reactivity toward CO oxidation. Unfortunately, nanocrystalline ceria powders predominantly expose their least reactive {111} surfaces, and preparation of polycrystalline materials with preferential exposure of specific reactive planes is very difficult. A correlation between sample morphology and overall catalyst performance has also recently been reported for samples of mesoporous ceria [12]. It was found that the conversion of different catalysts (measured by comparing T50 in light-off curves) against surface area has a maximum in the range of 900–1000 K, and this was correlated with changes in the morphology and in the characteristics of pore structure of the samples.

The work presented here further proceeds along these lines, by widening the investigation to the determination of specific activity under controlled kinetic conditions and by using different sets of starting materials with the aim of extending our conclusions to ceria powders, regardless of the preparation methods used. It was found that aging under air of polycrystalline ceria samples caused the rearrangement of crystallites, with loss of surface area and exposure of more reactive surfaces, which increases the specific activity in CO oxidation. However, because of the lower surface area of samples, the overall activity on a per-gram basis is lower. Other factors that can positively influence specific activity on large ceria crystallites are also discussed.

2. Experimental

Three different high-surface area samples of polycrystalline ceria powders were used as starting materials throughout this study. They were prepared according to different methods and are designated as CA, CB, and CC. Fresh CA sample (surface area 143 m^2/g) was prepared by moderate calcination (473 K) of cerium carbonate obtained from $Ce(NO_3)_3$ by precipitation with NH_4HCO_3. CB was prepared according to a process that involves the precipitation of a homogeneous acidic solution of cerium nitrate with a base. The filter cake is then washed with distilled water, followed by spray drying and calcination at 573 K. CC is a commercial sample of "stabilized ceria" prepared by a proprietary method and calcined at 773 K. The purity of samples was checked by chemical analysis; CA and CB samples had a purity greater than 99.8%, and the purity of the CC sample was greater than 99.4%. Main impurities for all samples were lanthanide oxides (La, Pr, Nd, Sm), alkaline earth oxides (CaO, MgO), and SiO_2. Traces of Na and Cl were also found.

We treated freshly prepared samples under air in a tubular furnace at different temperatures (up to 1073 K for a period of 2 h) in order to prepare a series of catalysts with increasing crystallite size and decreasing BET surface area. Textural and morphological properties of samples are summarized in Table 1. For brevity, samples are indicated followed by their calcination temperature: for example, CA calcined at 973 for 2 h is indicated as CA973.

Table 1
Textural and morphological characteristics of ceria samples

Sample	BET surface area (m^2/g)	Average pore diameter (nm)	Mean crystallite size (nm)	Specific rate at 543 K (mol m^{-2} h^{-1})×10^3
CA(473)	143	3.9	7	2.1
CA(673)	130	3.7	8	2.2
CA(773)	123	3.8	9	1.8
CA(873)	76	3.9	13	2.5
CA(973)	21	6.5	25	6.8
CA(1073)	10	12.2	51	8.8
CB(573)	100	4.9	10	5.9
CB(773)	95	4.7	11	6.2
CB(973)	19	6.7	21	6.9
CB(1073)	4	12.1	35	8.7
CC(773)	57	14.7	11	5.0
CC(873)	36	15.9	16	5.8
CC(973)	26	21.4	22	8.3
CC(1073)	12	27.7	41	9.0

BET surface area and pore size distribution were evaluated from the adsorption isotherm with a Sorptomatic 1990 porosimeter.

Structural features of the catalysts were investigated by X-ray diffraction. Spectra were recorded on a Philips X'Pert diffractometer (equipped with a real-time multiple strip detector) operated at 40 kV and 40 mA, with Ni-filtered Cu-K_α radiation. Spectra were collected with a step size of 0.02° and a counting time of 40 s per angular abscissa in the range of 20–145°. Rietveld refinement of the XRD pattern was performed by means of a GSAS-EXPGUI program. The mean crystallite size was estimated from the full width at half-maximum with the Scherrer formula.

TG analysis was carried out with a Q500 thermobalance (TA Instruments) under an air flow. Microstructural characterization by high-resolution transmission electron microscopy (HRTEM) was carried out with a JEOL 2010F instrument equipped with a field emission gun, which made it possible to achieve a point-to-point resolution of 0.19 nm and a resolution of 0.14 nm between lines. Samples were deposited directly on holey carbon-coated grids.

Catalytic activity measurements were carried out in a steady-state glass micro flow reactor ($\Phi = 6$ mm, $L = 300$ mm) operated in a temperature range of $300 \leqslant T \leqslant 1100$ K, with a total flow of 0.1 l/min. Typical feed conditions were as follows: CO (2%), O_2 (1%), and N_2 as diluent, with a GHSV of ca. 2×10^5 h^{-1}. Analysis of CO, O_2, and CO_2 was carried out under continuous conditions with an on-line infrared analyzer (ABB Uras-14 for CO, CO_2) and a paramagnetic O_2 analyzer (ABB Magnos-106). We collected conversion-versus-temperature curves (light-off profiles) by increasing the temperature at a rate of 10 K/min and monitoring conversion. Rate of CO oxidation has been determined at low conversion by assuming differential reactor conditions (i.e., conv. <5%); accuracy of rate values is within 15%, as determined by repeated measurements at fixed temperature. Reaction conditions were chosen to minimize the effect of mass and heat transfer phenomena. The

Table 2
Lattice parameter of CA sample calcined at different temperatures calculated by Rietveld refinement

Sample	Lattice parameter (Å)	Ce^{3+} (%)	Crystallite size (nm)
CA(473)	5.4222(2)	2.4	7
CA(673)	5.4165(3)	1.0	8
CA(773)	5.4137(1)	0.2	9
CA(873)	5.4112(1)	–	13
CA(973)	5.4109(1)	–	25
CA(1073)	5.4107(1)	–	51

absence of external and internal diffusion limitation was confirmed by experiments. We checked limitations in external transfer phenomena by measuring conversion at increasing W/F (catalyst weight/total flow) ratio and maintaining constant space velocity. A series of runs carried out under these conditions did not indicate any variation in conversion, thus ruling out any limiting effect of external diffusion phenomena. The absence of strong resistance to internal diffusion was determined by evaluation of the activation energy for the reaction in the temperature range investigated as reported in the following sections.

3. Results

3.1. Structural and textural properties

Powder X-ray diffraction data confirm in all samples the presence of crystalline CeO_2 as the only detectable phase. The formation of a cubic fluorite lattice of F*m3m* symmetry is always detected, with almost identical cell parameters. For CA samples a slight modification of cell parameter is observed after calcination at lower temperatures (Table 2), indicating the likely presence of some Ce^{3+} in samples with smaller crystallite size. This also agrees with the lattice expansion that has been observed in the fluorite-type lattice constant of CeO_2/CeO_{2-x} nanoparticles in the size range of 2–8 nm due to the presence of Ce^{3+} (either residual Ce^{3+} due to incomplete oxidation of oxide precursors and/or Ce^{3+} due to structural/quantum confinement or other physico-chemical effects [13]). For CB and CC samples lattice constants agree with a full CeO_2 stoichiometry at all calcination temperatures, in agreement with their crystallite size larger than 8 nm.

The average crystallite size as shown in Table 1 increases continuously with calcination temperature due to sintering. In accordance with this, larger particles display progressively lower BET surface area, which decreases continuously with temperature. Isotherms of type IV were obtained for all samples. From an examination of pore size distribution curves it can be concluded that for samples CA and CB, the largest area contribution is from pores less than 120 Å in diameter, whereas larger pores are found in sample CC regardless of calcination temperatures. Microporosity is absent in samples with a BET surface area lower than ca. 80 m^2/g.

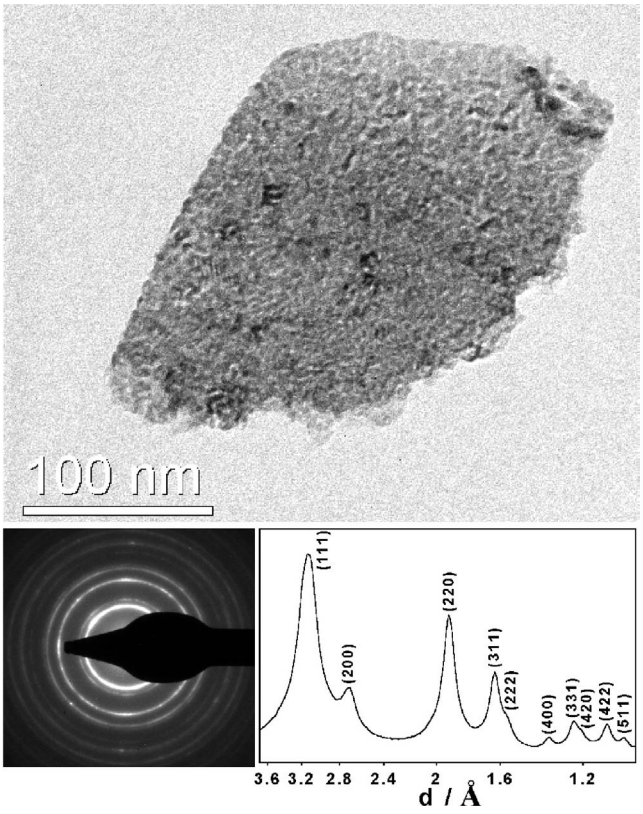

Fig. 1. Selected-area electron diffraction of a particle of high-surface area CB573 shown in bright-field. The averaged position and intensity of the rings in the ED pattern is also included and indexed according to the F*m3m* CeO_2 structure.

3.2. Surface morphology and exposed planes

Surface morphology of samples was investigated by transmission electron microscopy techniques. All samples displayed similar characteristics (sample CA was more difficult to study because of the presence of aggregates of ceria particles that were poorly resolved); we will comment here on images related to sample CB in the so-called fresh state (calcined at 573 K), after calcination at "low temperature" (CB773) and after calcination at "high temperature" (CB1073). TEM and electron diffraction analysis of the three samples revealed that they are constituted by CeO_2 crystallites. For fresh sample, electron diffraction patterns recorded in selected-area mode (SAED) in several regions show smooth rings, which indicate that the sample is polycrystalline and is constituted by very small crystallites. As a representative example, Fig. 1 shows an aggregate and its corresponding SAED pattern along with an integrated intensity-spacing profile. The reciprocal spacings of the electron diffraction pattern and their relative intensity confirm cerium dioxide as the only crystalline phase. High-resolution transmission electron microscopy (HREM) was used to accurately calculate the size of the crystallites by lattice-fringe analysis. The distribution of crystallite size is very homogeneous and is centered at ca. 7–8 nm, compared with a value of 10 nm calculated from XRD (Table 1).

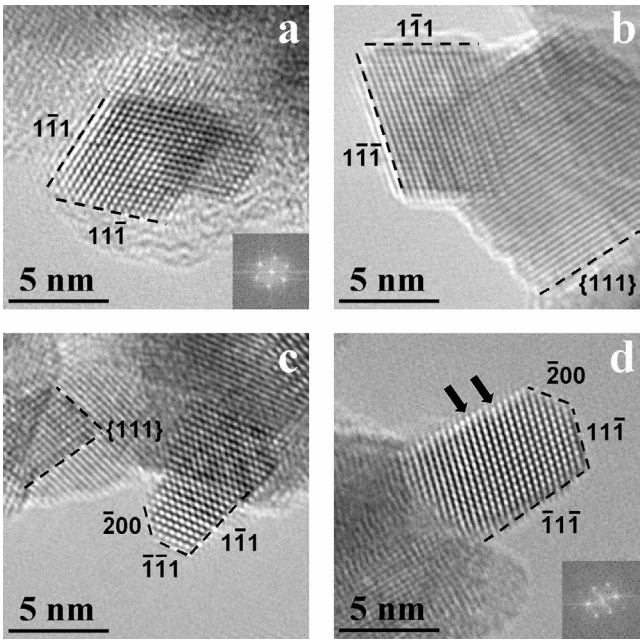

Fig. 2. Representative high-resolution TEM images of CB773 sample. Nanoparticles are oriented along the [011] crystallographic direction and show dominant {111}-type facet structures. The insets correspond to Fourier transform of individual domains in the HREM images. Arrows in (d) indicate surface steps.

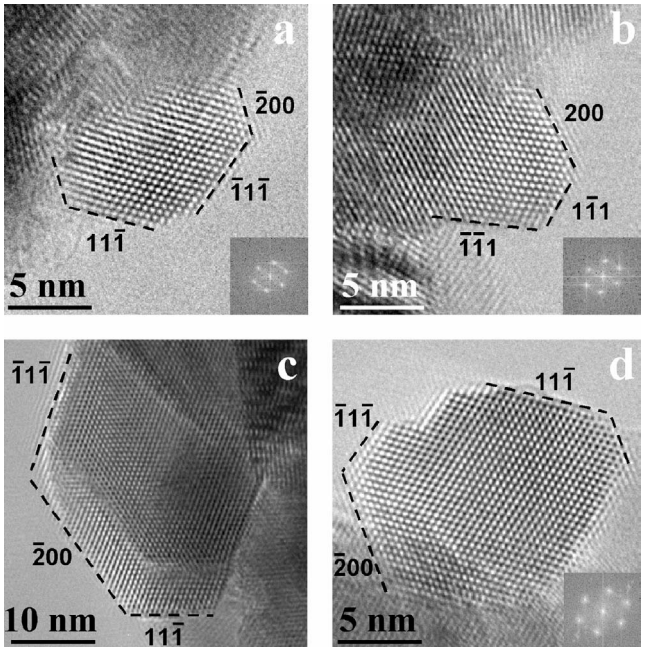

Fig. 3. Representative high-resolution TEM images of CB1073. Nanoparticles are oriented along the [011] crystallographic direction, showing {111}- and {100}-type facet structures.

It has been possible to characterize CB773 and the sample oxidized at 1073 K at the atomic scale by HREM over a large number of individual CeO_2 crystallites (more than 30 crystals for each sample). By identifying the lattice spacings and particle orientation, we determined the facets on the particle surfaces. Because of the agglomeration of particles, caution was taken to distinguish between lattice fringes of the same crystal and those originating from crystal overlapping.

Fig. 2 shows various individual, representative CeO_2 crystals in the CB773 sample (a–d). All of the crystallites are oriented along the [011] crystallographic direction. The labeling of the crystal planes for each particle is indicated in the figure. It is deduced that the dominant lattice fringes in all cases correspond to the {111} family, at 3.12 Å. The sharp faces of the CeO_2 crystals have very few surface steps and consist of symmetry-related {111}-type surfaces. The shape of most particles is compatible with an octahedron enclosed by eight {111} planes (Figs. 2a and b). These crystals exhibit also sharp tips, with only a few cerium atoms at the narrowest point. In addition to {111} planes, some particles of the fresh sample also exhibit {100}-type surfaces. This is illustrated in the crystallites depicted in Figs. 2c and d, where, in addition to {111} planes, there is also the presence of (200) planes at 2.71 Å. Occasional steps with {111}-type nanofaceting are indicated by arrows in Fig. 2d.

Typical images from the CeO_2 crystallites in the sample oxidized at 1073 K are displayed in Figs. 3a–d. Again, all of the crystallites are oriented along the [011] crystallographic direction. In these samples the CeO_2 crystallites probably agglomerate by minimizing the interface energy with the formation of a lattice-matched coherent interface [14], which may explain the observed distribution of crystallites with a preferred orientation of [011]. In this case, extensive {100} facets are encountered in addition to {111} planes. The treatment under oxygen results in the truncation of the sharp tips between two {111}-type surfaces along the perpendicular [100] crystallographic direction, originating the (200) planes depicted in Fig. 3. This is consistent with the truncated octahedral shape of the crystallites, which is the new surface of the {100}-type.

3.3. Catalytic tests

A representative series of curves showing the effect of calcination temperature on CO conversion under stationary conditions over CA samples is presented in Fig. 4. A typical smooth light-off behavior is observed; the shape of the curves shows that conversion is negligible at low temperature ($T < 500$ K), and in all cases investigated the onset of activity starts at 500–600 K, with total conversion approached at ca. 750 K for most samples. Overall activity on a per-gram basis follows the inverse order of calcination temperatures, where the sample calcined at high temperatures is the least active (i.e., activity of CA473 > CA573 > ⋯ > CA1073).

We made an accurate determination of specific activity by measuring the rate of CO oxidation at low conversions (from the conversion-vs.-temperature curves), assuming differential reactor conditions, under a kinetically controlled regime. The advantage over a measurement carried out by

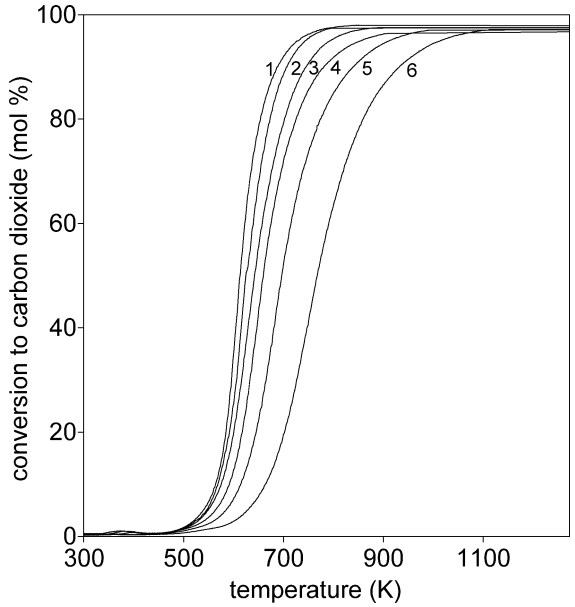

Fig. 4. Light off curves of CO oxidation for CA samples calcined at increasing temperatures (1, CA473; 2, CA573; . . .; 6, CA1073). For conditions see experimental section.

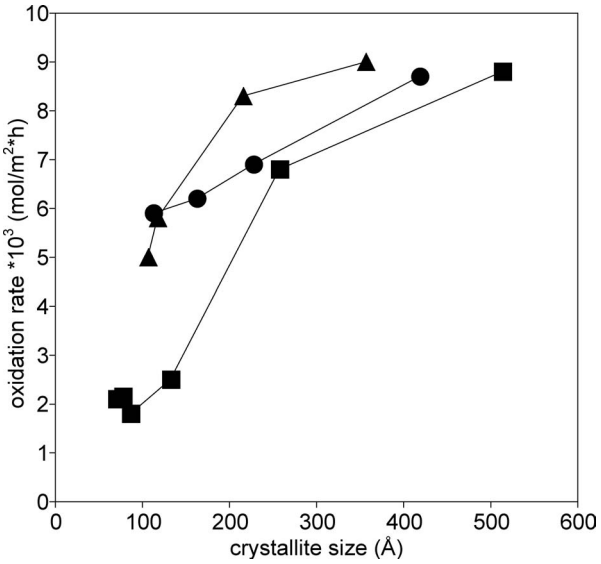

Fig. 5. Specific rate of CO oxidation calculated at 543 K against crsyatllite size for CA (■), CB (▲), and CC (●) samples.

evaluation of T50 only is the possibility of calculating the specific turnover rate, which excludes the contribution of surface area to the measured values. In addition, the rate is measured under a kinetic regime, since conversion at T50 is sometimes influenced by diffusion and mass-transfer phenomena [15]. Fig. 5 displays rate data against crystallite size; the overall picture is now more clear; specific activity shows a marked dependence on the crystallite size, regardless of the preparation history of the sample. Particularly in the size range from 10 to 40 nm, the activity is strongly dependent on crystallite size, whereas the increase in activity for particles larger than 40 nm seems to reach limiting values, at least for samples CA and CB.

4. Discussion

The oxidation of carbon monoxide over CeO_2-based materials under aerobic and anaerobic conditions has been the subject of intense investigation in recent years [6,16–19]. It is generally accepted that the prevalent mechanism involves a redox Mars–van Krevelen-type reaction in which CO reacts with surface ceria, forming an oxygen vacancy, which is then replenished by gas-phase oxygen. Formation and desorption of CO_2 complete the cycle. The presence of carbonate-like adsorbates as intermediates before CO_2 desorption is a possibility, especially under cycled feedstream conditions [3,6,20,21]. It is in fact reported that carbonate-like or inorganic carboxylate-like complexes of CO are formed on a CeO_2 surface when it is exposed to a CO atmosphere [22–24]. In addition, it is also known that the adsorption behavior of CO on ceria surfaces is strongly related to the nature of the surfaces used in the experiments [25]; in particular, whereas only weak adsorption has been predicted for the {111}-type surface, both weak and strong adsorption is detected on the {110}-type surface, giving rise to carbonate formation. The different reactivity of CO with exposed surfaces of ceria is also the result of the different stabilities of exposed planes. It is known from the theoretical molecular mechanic method that the stabilities of three low-index planes in the ceria fluorite cubic structure follow the order {111} > {110} > {100} [8–10,26], with the consequence that formation of anionic vacancies is easier in {110} and {100} surfaces. Therefore, since less energy is required to form an oxygen vacancy on these surfaces, it is much easier to accommodate here reaction with CO. The main consequence of this finding is that the redox reactivity of ceria (especially toward CO) might strongly depend on the type and amount of surfaces exposed to the gas phase. As a matter of fact, it has recently been demonstrated that nanorods preferentially exposing the unusually reactive {100} and {110} planes have a lower light-off temperature for CO oxidation than their counterpart irregular nanoparticles [11].

In polycrystalline ceria the situation is much more complex, since preferential exposure of different planes is difficult to control, although it has been found that ceria surfaces consisting exclusively of {111} lattice planes, upon annealing at 1073 K, form a well-defined portion of {100} surfaces [27]. Changes in surface morphology and in the pore structure were also recently shown to be the origin of different activities of samples of mesoporous ceria [15]. Also in this case, the activity data are compared by evaluation of T50 in light-off curves carried out at different space velocities, and the shape of light-off curves cannot exclude an effect of mass transport limitation within pores, which poses a few limits on the generalization of the conclusions reached in this investigation. Our study reveals that preferential exposure of specific surfaces upon treatment under

Table 3
Activation energy calculated in the range of temperature 500–573 K

Calcination temperature	E_{att} (kcal/mol)		
(K)	CA	CB	CC
473	15.1	–	–
573	–	16.4	16.4
673	14.3	–	–
773	14.5	15.7	17.4
873	12.1	–	18.1
973	15.6	14.0	17.8
1073	13.7	15.1	13.6

oxidizing conditions is found also in pure crystalline ceria, regardless of the preparation method used. Although measured on a qualitative basis, this finding is supported by the large (and statistically significant) number of individual crystallites that were examined. The above HRTEM studies indicate that CeO_2 particles after calcination at high temperature expose, in addition to {111} planes, well-defined and less stable {100} planes, whereas in CeO_2 not subjected to high temperature treatments, the most stable {111} planes are predominantly exposed. In addition, at calcination temperatures above 773 K, the change in exposed surfaces results in an increase in specific rate of CO oxidation.

The observed increase in specific reaction rate value upon calcination might be the consequence of several physicochemical modifications of the surface of ceria crystallites. We will try to present evidence here that there is a relation between preferential plane exposure and increase in CO oxidation rate, and at the same time we will attempt to exclude the presence of other phenomena.

We have found that the strong surface area loss that follows calcination is always accompanied by an increase in mean particle diameter and average pore size. This can affect intra- and extra-particle diffusion resistance. In particular, resistance to internal pore diffusion in high-surface area particles would have the effect of reducing the apparent specific reaction rate in materials that have a relevant fraction of surface area constituted by micro pores. The overall effect would be an increase in specific reaction rate after high calcination temperatures, due to a drop in internal pore diffusion. A quite general and simple method for excluding any intra-particle diffusional limitation is the calculation of activation energy in the range of temperature of interest [28]. Table 3 summarizes the results of an internal diffusion test: they show that regardless of the sample used, the activation energy does not depend on calcination temperatures. The values found are around 14–16 kcal/mol, close to those reported for CO oxidation under similar conditions [29,30]. This rules out the possibility that measurements of specific rate values were influenced by internal porosity of our samples.

The presence of impurities in samples calcined at low temperature is another matter that deserves further investigation. Because of the preparation method used in our study,

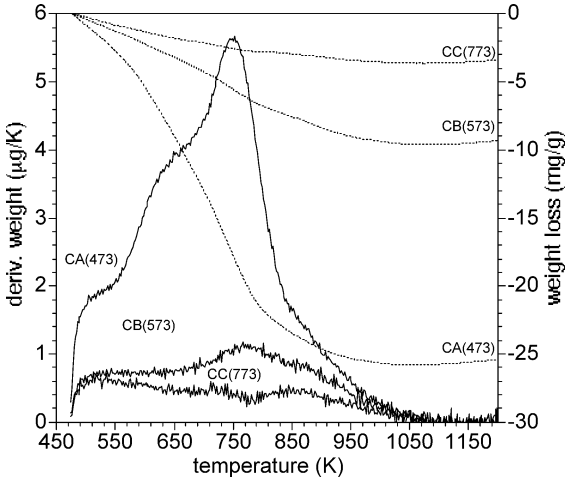

Fig. 6. Weight loss and derivative weight profiles as measured with a TG experiment conducted by heating under air fresh samples from 473 to 1273 K at 10 K/min. Dotted line (weight loss, right axis) and solid line (derivative weight, left axis).

the presence of residual carbonates and nitrates is a possibility in samples calcined at low temperature (especially carbonates in sample CA). Fig. 6 shows a TG analysis of the three ceria samples conducted under air, which indicates a significant weight loss for the CA sample between 500 and 850 K, corresponding to the decomposition of surface carbonates and minor desorption features for CB and CC samples. For calcination temperatures of 900–1100 K, in the region where CO oxidation activity is strongly enhanced, no significant weight loss is detected, thus ruling out a possible role of desorption of surface impurities in the increase of activity observed on samples calcined at high temperatures. In a plot of the first derivative of the weight loss signal, several contributions are indicated at low temperatures, with a maximum for CA and CB samples at ca. 760 K, and a broad shoulder above this temperature. This is likely to be associated with elimination of bulk ceria carbonates that need relatively high calcination temperatures [3]. Desorption of carbonates, especially for CA samples, does not seem to influence the specific rate of CO oxidation, as inferred from the fact that no relevant changes in activity are observed in CA samples calcined in the range of 470–800 K (the samples have higher surface area), where most of the surface carbonate decomposition takes place. However, one thing that can explain the difference in activity of CA(473–873) and CB/CC samples is the possibility that desorption of carbonates indirectly affects the activity by blocking the development of {100} faces. This hypothesis, suggested by a referee, can be supported by the fact that activity in the CA sample sharply increased *after* desorption of carbonates at high temperatures (most likely bulk carbonates) but is not affected *during* desoprtion of carbonates at lower temperatures.

Stoichiometry of ceria particles should also be taken into account to properly address the issue of specific activity in

CO oxidation. We have found that in the CA sample, the lattice parameters of smaller ceria particles (CA473–CA773) agree with the presence of some Ce^{3+} in the lattice. It is known that nanoparticles of ceria can strongly deviate from stoichiometry because of the presence of Ce^{3+} [14,31,32], and it is also reported that in nanocrystalline ceria powder the thermodynamics and kinetics of reduction may strongly vary from what is generally observed in bulk ceria [33]. The presence of Ce^{3+} and associated surface vacancies would lower the number of active sites for CO reaction, thus decreasing specific activity calculated on a square-meter basis. The amount of Ce^{3+} found in our samples, keeping also in mind that more surface Ce^{3+} could have escaped XRD detection, is localized on samples with a small crystal size and showing almost constant activity. No changes in stoichiometry are observed in any samples where changes of activity were detected. In any case, for the majority of samples, the atmosphere of reaction should guarantee the presence of stoichiometric ceria at the reaction temperature.

Having excluded several major possible explanations of the increase in the CO oxidation rate against calcination temperature, we might now rationalize this behavior in terms of (i) preferential formation of more reactive {100} planes after calcination of crystalline ceria powders in the range of temperature between 573 and 1073 K and (ii) particularly favorable energetics expected for CO oxidation over these reactive surfaces. The favorable formation of {100}-type surfaces upon treatment at high temperature under O_2-containing atmospheres has already been reported for oriented CeO_2 films [27]. In the case of polycrystalline ceria, some conflicting observations were found in the literature: it is known that CeO_2 particles preferentially expose the {111} planes, which is the one of lowest energy [1]. In agreement with this, HRTEM studies of CeO_2 reveal that high-surface-area samples show grains oriented to expose predominantly {111} planes. This preferential exposure was reported to become dramatically apparent after mild oxidation at 773 K compared with fresh samples [34], thus excluding in this study {100} faceting. Conversely, Lunberg et al. [10] reported that from calcination temperatures of 773 to 973 K, {100} facets were clearly present, and their formation was attributed to calcination, since at $T < 773$ K no {100} facets were observed. In this work, an increase in {100} facets is progressively observed after calcination of polycrystalline ceria at $T > 773$ K. Therefore, it might be concluded that, excluding a transition region around 773 K, temperatures higher than 773 K favor the exposure of more reactive planes. To address the second point raised above, we suggest that improved activity of CeO_2 after calcination is due to the greater capacity of CeO_2 {100}-type surfaces compared with {111} to help CO oxidation by supplying oxygen and changing valence. A similar mechanism of action was described earlier with Pt(111) on ordered (111) CeO_2 film [35] and on CuO supported on CeO_2(100) surfaces [27]. In these cases CO oxidation benefits from the presence of the redox of ceria, which is facilitated when more reactive planes are exposed. In addition, although specifically supported for {110} and not for {100} surfaces, a stronger interaction of CO with this surface might lead to easier formation of carbonate-like adsorbates, which is a key step in carbon monoxide oxidation over ceria particles.

In summary, evidence is presented that highlights the role of reactive surfaces in CO oxidation over different samples of polycrystalline ceria powders prepared by conventional methods. These samples, in a fresh state, expose preferentially the more stable {111}-type surfaces, and after thermal treatment more reactive surfaces become visible, at the expense of a drop in surface area. Therefore, observations recently reported for 1D ceria samples obtained by more sophisticated techniques have been extended to conventionally prepared polycrystalline ceria samples with catalytic data recorded under conditions that were determined to be free from mass transport limitations. The possibility of exposing more reactive surfaces by nonconventional techniques, thus preserving high surface area, would therefore represent a key and challenging step in the design of ceria-based catalysts with enhanced redox properties.

Acknowledgments

The authors are grateful to Grace Davison (USA) and Treibacher (A) for providing starting materials used in this study. We also thank FIRB and PRIN projects for financial support and Dr. Roberta Di Monte (University of Trieste) for carrying out pore size measurements. J.Ll. is grateful to MCYT and DURSI.

References

[1] A. Trovarelli (Ed.), Catalysis by Ceria and Related Materials, Imperial College Press, London, 2002, pp. 1–528.
[2] R. Di Monte, J. Kaspar, Top. Catal. 28 (2004) 47.
[3] A. Trovarelli, Catal. Rev. Sci. Eng. 439 (1996) 38.
[4] M.F. Milkes, P. Hayden, A.K. Bhattacharya, J. Catal. 219 (2003) 295.
[5] W. Liu, M. Flytzani-Stephanopoulos, J. Catal. 153 (1995) 304.
[6] Y. Madier, C. Descorme, A.M. LeGovic, D. Duprez, J. Phys. Chem. B 103 (1999) 10999.
[7] R.H. Nibbelke, A.J.L. Nievergeld, J.H.B.H. Hoebnik, G.B. Marin, Appl. Catal. B: Environ. 19 (1998) 245.
[8] T.X.T. Sayle, S.C. Parker, C.R.A. Catlow, Surf. Sci. 316 (1994) 329.
[9] J.C. Conesa, Surf. Sci. 339 (1995) 337.
[10] M. Baudin, M. Wojcik, K. Hermansson, Surf. Sci. 468 (2000) 51.
[11] K. Zhou, X. Wang, X. Sun, Q. Peng, Y. Li, J. Catal. 229 (2005) 206.
[12] M. Lundberg, B. Skarman, L.R. Wallenberg, J. Micropor. Mesopor. Mater. 69 (2004) 187.
[13] M.D. Hernandez-Alonso, A.B. Hungria, A. Martinez-Arias, J.M. Coronado, J.C. Conesa, J. Soria, M. Fernandez-Garcia, Phys. Chem. Chem. Phys. 6 (2004) 3524.
[14] Z.I. Wang, X. Feng, J. Phys. Chem. B 107 (2003) 13563.
[15] F. Duprat, Chem. Eng. Sci. 57 (2002) 901.
[16] M. Boaro, C. de Leitenburg, G. Dolcetti, A. Trovarelli, J. Catal. 193 (2000) 338.
[17] R. Rajasree, J.H.B.J. Hoebink, J.C. Schouten, J. Catal. 223 (2004) 36.

[18] P.S. Lambrou, C.N. Costa, S.Y. Christou, A.M. Efstathiou, Appl. Catal. B: Environ. 54 (2004) 237.
[19] A. Martorana, G. Deganello, A. Longo, A. Prestianni, L. Lotta, A. Macaluso, G. Pantaleo, A. Balerna, S. Mobilio, J. Solid State Chem. 177 (2004) 1268.
[20] C. Mondelli, V. Dal Santo, A. Trovarelli, M. Boaro, A. Fusi, R.Psaro, S. Recchia, Catal. Today (2005), in press.
[21] M. Boaro, F. Giordano, S. Recchia, V. Dal Santo, M. Giona, A. Trovarelli, Appl. Catal. B: Environ. 52 (2004) 225.
[22] D.R. Mullins, S.H. Overbury, J. Catal. 188 (1999) 340.
[23] C. Binet, A. Badri, M. Boutonnet-Kizling, J.C. Lavalley, J. Chem. Soc. Faraday Trans. 90 (1994) 1023.
[24] F. Bozon-Verduraz, A. Bensalem, J. Chem. Soc. Faraday Trans. 90 (1994) 653.
[25] Z. Yang, T.K. Woo, K. Hermansson, Chem. Phys. Lett. 396 (2004) 384.
[26] D.C. Sayle, S.A. Maicaneanu, G.W. Watson, J. Am. Chem. Soc. 124 (2002) 11429.
[27] B. Skarman, L.R. Wallenberg, P.-O. Larsson, A. Andersson, J.-O. Bovin, S.N. Jacobsen, U. Helmersson, J. Catal. 181 (1999) 6.
[28] O. Levenspiel, Chemical Reaction Engineering, second ed., Wiley, New York, 1972.
[29] A. Bielanski, J. Haber, Oxygen in Catalysis, Dekker, New York, 1991.
[30] S.J. Schmieg, D.N. Belton, Appl. Catal. B: Environ. 6 (1995) 127.
[31] S. Tsunekawa, K. Ishikawa, Z.Q. Li, Y. Kawazoe, A. Kasuya, Phys. Rev. Lett. 85 (2000) 3440.
[32] F. Zhang, Q. Jin, S.W. Chan, J. Appl. Phys. 95 (2004) 4321.
[33] F. Giordano, A. Trovarelli, C. de Leitenburg, M. Giona, J. Catal. 193 (2000) 273.
[34] Z.C. Kang, L. Eyring, J. Alloys Comp. 249 (1992) 206.
[35] C. Hardacre, R.M. Ormerod, R.M. Lambert, J. Phys. Chem. 98 (1994) 10901.